Available online at www.sciencedirect.com
SCIENCE DIRECT®
Computers and Structures 83 (2005) 463–478
Computers & Structures
www.elsevier.com/locate/compstruc

Simulating the dynamics of fluid–ellipsoid interactions

Tsorng-Whay Pan [a,*], Daniel D. Joseph [b], Roland Glowinski

[a] University of Houston, Department of Mathematics, Houston, TX 77204-3008, USA
[b] Department of Aerospace Engineering and Mechanics, University of Minnesota, MN 55455, USA

Accepted 19 August 2004
Available online 21 December 2004

Abstract

We present the simulation of the dynamics of fluid–ellipsoid interactions in a narrow channel filled with a Newtonian fluid, using a Lagrange multiplier based fictitious domain methodology. As expected, a settling ellipsoid turns its broadside perpendicular to the stream main direction and the center of mass moves to the central axis of the channel. For two ellipsoid cases, we have obtained two kinds of interactions between two ellipsoids: (1) they settle side-by-side and interact with each other periodically; (2) they keep moving around each other and stay together. We also found that the length of longest axis plays an important role for these interactions.

Keywords: Particulate flow; Finite element methods; Operator-splitting methods; Fictitious domain methods

1. Introduction

The orientation of symmetric long body, e.g., ellipsoid and truncated cylinder, settling in liquids of different nature is a fundamental issue in many problems of practical interest (see, e.g., [1], and the references therein). In the past decade, more and more researchers have developed numerical methods for the direct simulation of fluid/particle interaction, e.g., see Refs. [2–13] and the references therein for more details. In this article we first discuss the generalization of a Lagrange multiplier based fictitious domain method [9,10] to the simulation of the motion of particles of general shape in a Newtonian fluid. Unlike the cases where the particles are spheres, we attach two points to each particle and move them according to the rigid-body motion of the particle. The equations describing the motion of these two points are solved by a distance preserving scheme so that rigidity can be maintained. Then we apply the above methodology to simulate the settling of ellipsoids in a narrow channel filled with a Newtonian fluid. As expected, a settling ellipsoid turns its broadside perpendicular to the stream main direction and the center of mass moves toward the central axis of the channel. For two ellipsoid cases, we have obtained two kinds of interactions. When initially placed side-by-side, they sediment side-by-side and interact with each other periodically. But with short long axis, the interaction between two ellipsoids is weaker. When releasing initially one on top of the other, we have observed that two ellipsoids keep moving around each other and stay together while they are settling down in the channel. Depending on the length of the longest axis, they can either interact at one side of the channel or interact and oscillate between two sides of the channel. The simulations discussed in this article concern fluid-rigid solid interactions. More general situations are discussed in, e.g., [14,15], where the

* Corresponding author. Tel: +713 743 3448; fax: +713 743 3505.
E-mail address: pan@math.uh.edu (T.-W. Pan).

0045-7949/$ - see front matter © 2004 Elsevier Ltd. All rights reserved.
doi:10.1016/j.compstruc.2004.08.019

case of elastic solids is also considered (see also the references therein).

2. A model problem and fictitious domain formulation for three-dimensional particulate flow

To perform the *direct numerical simulation* of the interaction between particles and fluid, we have developed a methodology which combines a distributed Lagrange multiplier based fictitious domain (also called domain embedding) method with operator splitting methods [9,10,16–18]. This approach (or closely related ones derived from it) has been used by other investigators (e.g., [12,19–21]). We are going to recall the ideas at the basis of the above methodology by considering the motion of a single particle in a Newtonian viscous incompressible fluid (of density ρ_f and viscosity ν_f) under the effect of gravity; actually, the generalization to a thousand of *spherical* particles in 3-D and 10,000 *circular* particles in 2-D is possible as shown in [10,22,23]. For the situation depicted in Fig. 1 (for non-spherical particle cases), the flow is modeled by the Navier–Stokes equations, namely, (with obvious notation)

$$\rho_f\left[\frac{\partial \mathbf{u}}{\partial t}+(\mathbf{u}\cdot\nabla)\mathbf{u}\right]-\nu_f\Delta\mathbf{u}+\nabla p = \rho_f\mathbf{g} \quad \text{in } \Omega\setminus\overline{B(t)},\quad 0<t<T, \tag{1}$$

$$\nabla\cdot\mathbf{u}=0 \quad \text{in } \Omega\setminus\overline{B(t)},\quad 0<t<T, \tag{2}$$

$$\mathbf{u}(0)=\mathbf{u}_0(\mathbf{x}) \quad (\text{with } \nabla\cdot\mathbf{u}_0=0), \tag{3}$$

$$\mathbf{u}=\mathbf{g}_0 \quad \text{on } \Gamma\times(0,T), \text{ with } \int_\Gamma \mathbf{g}_0\cdot\mathbf{n}\,d\Gamma=0, \tag{4}$$

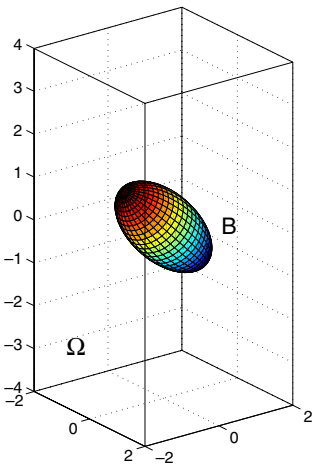

Fig. 1. The flow region with one particle.

where $\Gamma=\partial\Omega$, $\mathbf{g}$ denotes gravity and $\mathbf{n}$ is the unit normal vector pointing outward to the flow region. We assume a *no-slip condition* on $\gamma(=\partial B)$. The motion of particle B satisfies the Euler–Newton's equations, namely

$$\mathbf{v}(\mathbf{x},t)=\mathbf{V}(t)+\boldsymbol{\omega}(t)\times\overrightarrow{\mathbf{G}(t)\mathbf{x}}, \quad \forall\{\mathbf{x},t\}\in\overline{B(t)},\quad 0<t<T, \tag{5}$$

$$\frac{d\mathbf{G}}{dt}=\mathbf{V}, \tag{6}$$

$$M_p\frac{d\mathbf{V}}{dt}=M_p\mathbf{g}+\mathbf{F}_H+\mathbf{F}^r, \tag{7}$$

$$\frac{d(\mathbf{I}_p\boldsymbol{\omega})}{dt}=\mathbf{T}_H+\vec{\mathbf{G}}\vec{\mathbf{x}}_r\times\mathbf{F}^r, \tag{8}$$

with the resultant and torque of the hydrodynamical forces given by, respectively,

$$\mathbf{F}_H=-\int_\gamma \boldsymbol{\sigma}\mathbf{n}\,d\gamma,\ \mathbf{T}_H=-\int_\gamma \vec{\mathbf{G}}\vec{\mathbf{x}}\times\boldsymbol{\sigma}\mathbf{n}\,d\gamma \tag{9}$$

with $\boldsymbol{\sigma}=\nu_f\ (\nabla\mathbf{u}+\nabla\ \mathbf{u}\ ^t)-p\,\mathbf{I}$. Relations (1)–(9) are completed by the following initial conditions

$$\mathbf{G}(0)=\mathbf{G}_0,\quad \mathbf{V}(0)=\mathbf{V}_0,\quad \boldsymbol{\omega}(0)=\boldsymbol{\omega}_0,\quad B(0)=B_0. \tag{10}$$

Above, M_p, $\mathbf{I}_p$, $\mathbf{G}$, $\mathbf{V}$ and $\boldsymbol{\omega}$ are the mass, inertia, center of mass, velocity of the center of mass and angular velocity of particle B, respectively. In (8) we found preferable to deal with the *kinematic angular momentum* $\mathbf{I}_p\boldsymbol{\omega}$ making the formulation more conservative. In order to avoid particle-particle and particle-wall penetration which can happen in the numerical simulation, we have introduced a artificial short-range repulsion force $\mathbf{F}^r$ in (7), which becomes active when the shortest distance between two (convex) particles or between (convex) particle and wall is less than a prechosen distance (for more details, see, e.g., [9] and [10]; see also [24] for another approach) and then a torque in (8) acting on the point $\mathbf{x}_r$ where $\mathbf{F}^r$ applies on B. For non-convex particles, we can apply similar approach to activate the short-range repulsion force $\mathbf{F}^r$.

To solve system (1)–(10) we can use, for example, *Arbitrary Lagrange–Euler* (*ALE*) methods as in [5–7], or *fictitious domain methods*, which allow the flow calculation on a fixed grid, as in [9,10,16–18]. The fictitious domain methods that we advocate have some common features with the *immersed boundary method* of Ch. Peskin (see, e.g., Refs. [25–27]) but also some significant differences in the sense that we take systematically advantage of *distributed Lagrange multipliers* to force the rigid body motion inside the particle. As with the methods in [25–27], our approach takes advantage of the fact that the flow can be computed on a grid which

does not have to vary in time, a substantial simplification indeed.

The principle of fictitious domain methods is simple. It consists of

- Filling the particles with a fluid having the same density and viscosity as the surrounding one.
- Compensating the above step by introducing, in some sense, an *anti-particle* of mass $(-1)M_p\frac{\rho_f}{\rho_s}$ and inertia $(-1)\mathbf{I}_p\frac{\rho_f}{\rho_s}$, taking into account the fact that any rigid body motion $\mathbf{v}(\mathbf{x},t)$ verifies $\nabla\cdot\mathbf{v}=0$ and $\mathbf{D}(\mathbf{v})=\mathbf{0}$ (ρ_s: particle density).
- Finally, imposing the rigid body velocity on $\overline{B(t)}$, namely

$$\mathbf{v}(\mathbf{x},t)=\mathbf{V}(t)+\boldsymbol{\omega}(t)\times\overrightarrow{\mathbf{G}(t)\mathbf{x}},\quad \forall\mathbf{x}\in\overline{B(t)},\quad \forall t\in(0,T), \tag{11}$$

via a Lagrange multiplier $\boldsymbol{\lambda}$ supported by $\overline{B(t)}$. Vector $\boldsymbol{\lambda}$ forces rigidity in $B(t)$ in the same way that ∇p forces $\nabla\cdot\mathbf{v}=0$ for incompressible fluids.

We obtain then an equivalent formulation of (1)–(10) defined on the whole domain Ω, namely

For a.e. $t>0$, find $\{\mathbf{u}(t),p(t),\mathbf{V}(t),\mathbf{G}(t),\boldsymbol{\omega}(t),\boldsymbol{\lambda}(t)\}$ such that

$$\mathbf{u}(t)\in\mathbf{W}_{\mathbf{g}_0}(t),\quad p(t)\in L^2_0(\Omega),\quad \mathbf{V}(t)\in\mathbb{R}^3,\quad \mathbf{G}(t)\in\mathbb{R}^3,\quad \boldsymbol{\omega}(t)\in\mathbb{R}^3,\quad \boldsymbol{\lambda}(t)\in\Lambda(t) \tag{12}$$

and

$$\begin{cases}\rho_f\int_\Omega\left[\frac{\partial\mathbf{u}}{\partial t}+(\mathbf{u}\cdot\nabla)\mathbf{u}\right]\cdot\mathbf{v}\,d\mathbf{x}-\int_\Omega p\nabla\cdot\mathbf{v}\,d\mathbf{x}+\nu_f\int_\Omega\nabla\mathbf{u}:\nabla\mathbf{v}\,d\mathbf{x}\\ \quad-\langle\boldsymbol{\lambda},\mathbf{v}-\mathbf{Y}-\boldsymbol{\theta}\times\overrightarrow{\mathbf{G}\mathbf{x}}\rangle_{\Lambda(t)}+\left(1-\frac{\rho_f}{\rho_s}\right)\left[M_p\frac{d\mathbf{V}}{dt}\cdot\mathbf{Y}\right.\\ \quad\left.+\frac{d(\mathbf{I}_p\boldsymbol{\omega})}{dt}\cdot\boldsymbol{\theta}\right]-\mathbf{F}^r\cdot\mathbf{Y}-\overrightarrow{\mathbf{G}x_r}\times\mathbf{F}^r\cdot\boldsymbol{\theta}\\ \quad=\left(1-\frac{\rho_f}{\rho_s}\right)M_p\mathbf{g}\cdot\mathbf{Y}+\rho_f\int_\Omega\mathbf{g}\cdot\mathbf{v}\,d\mathbf{x},\\ \forall\mathbf{v}\in(H^1_0(\Omega))^3,\quad\forall\mathbf{Y}\in\mathbb{R}^3,\quad\forall\boldsymbol{\theta}\in\mathbb{R}^3,\end{cases} \tag{13}$$

$$\int_\Omega q\nabla\cdot\mathbf{u}(t)\,d\mathbf{x}=0,\quad\forall q\in L^2(\Omega), \tag{14}$$

$$\frac{d\mathbf{G}}{dt}=\mathbf{V}, \tag{15}$$

$$\langle\boldsymbol{\mu},\mathbf{u}(t)-\mathbf{V}(t)-\boldsymbol{\omega}(t)\times\overrightarrow{\mathbf{G}(t)\mathbf{x}}\rangle_{\Lambda(t)}=0,\quad\forall\boldsymbol{\mu}\in\Lambda(t), \tag{16}$$

$$\mathbf{V}(0)=\mathbf{V}_0,\quad\boldsymbol{\omega}(0)=\boldsymbol{\omega}_0,\quad\mathbf{G}(0)=\mathbf{G}_0,\quad B(0)=B_0, \tag{17}$$

$$\mathbf{u}(\mathbf{x},0)=\tilde{\mathbf{u}}_0(\mathbf{x})=\begin{cases}\mathbf{u}_0(\mathbf{x}), & \forall\mathbf{x}\in\Omega\setminus\overline{B(0)},\\ \mathbf{V}_0+\boldsymbol{\omega}_0\times\overrightarrow{\mathbf{G}_0\mathbf{x}}, & \forall\mathbf{x}\in\overline{B(0)},\end{cases} \tag{18}$$

with the following functional spaces

$$\mathbf{W}_{\mathbf{g}_0}(t)=\{\mathbf{v}\mid\mathbf{v}\in(H^1(\Omega))^3,\quad\mathbf{v}=\mathbf{g}_0(t)\text{ on }\Gamma\},$$
$$L^2_0(\Omega)=\left\{q\mid q\in L^2(\Omega),\int_\Omega q\,d\mathbf{x}=0\right\},$$
$$\Lambda(t)=(H^1(B(t)))^3.$$

Various examples for $\langle\cdot,\cdot\rangle_{\Lambda(t)}$ in (13) and (16) are given in [10,28, Chapter 8].

Remark 1. The second gravity term in the right-hand-side of the (13) can be combined with the pressure. Hence in the following, we will not use this term anymore.

In (12)–(18), only the center of mass, the translation velocity of the center of mass and the angular velocity of the particle are considered. Knowing these two velocities and the center of mass of the particle, one is able to translate and rotate the particle in space by tracking two extra points $\mathbf{x}_1$ and $\mathbf{x}_2$ in each particle, which follow the rigid body motion

$$\frac{d\mathbf{x}_i}{dt}=\mathbf{V}(t)+\boldsymbol{\omega}(t)\times\overrightarrow{\mathbf{G}(t)\mathbf{x}_i},\quad\mathbf{x}_i(0)=\mathbf{x}_{i,0},\quad i=1,2. \tag{19}$$

In practice we shall track two orthogonal normalized vectors rigidly attached to the body B and originating from the center of mass G.

3. Time and space discretization

3.1. Lie's scheme: a first order operator-splitting scheme

Many operator-splitting schemes can be applied to problem (12)–(19). One of the advantage of operator-splitting schemes is that we can decouple difficulties such as (i) the incompressibility condition, (ii) the non-linear advection term, and (iii) the rigid body motion, so that each one of them can be handled separately, and in principle optimally. Let Δt be a time discretization step and $t^{n+s}=(n+s)\Delta t$. The Lie's scheme is a *first order* operator-splitting scheme [29], which, when applied to problem (12)–(19), yields:

$$\mathbf{u}^0=\tilde{\mathbf{u}}_0,\quad\mathbf{G}^0=\mathbf{G}_0,\quad\mathbf{V}^0=\mathbf{V}_0,\quad\boldsymbol{\omega}^0=\boldsymbol{\omega}_0,$$
$$\mathbf{x}_1^0=\mathbf{x}_{1,0},\quad\mathbf{x}_2^0=\mathbf{x}_{2,0}\text{ given;} \tag{20}$$

for $n \geqslant 0$, $\mathbf{u}^n(\simeq \mathbf{u}(t^n))$, $\mathbf{G}^n$, V^n, $\boldsymbol{\omega}^n$, $\mathbf{x}_1^n$ and $\mathbf{x}_2^n$ being known, we first compute $\mathbf{u}^{n+1/6}$, $p^{n+1/6}$ via the solution of

$$\begin{cases} \rho_f \int_\Omega \frac{\partial \mathbf{u}}{\partial t} \cdot \mathbf{v}\,d\mathbf{x} - \int_\Omega p \nabla \cdot \mathbf{v}\,d\mathbf{x} = 0, \quad \forall \mathbf{v} \in (H_0^1(\Omega))^3, \\ \quad \text{a.e. on } (t^n, t^{n+1}), \\ \int_\Omega q \nabla \cdot \mathbf{u}\,d\mathbf{x} = 0, \quad \forall q \in L^2, \\ \mathbf{u}(t^n) = \mathbf{u}^n, \\ \mathbf{u}(t) \in (H^1(\Omega))^3, \mathbf{u}(t) = \mathbf{g}(t^{n+1}) \\ \quad \text{on } \Gamma \times (t^n, t^{n+1}), p(t) \in L_0^2, \end{cases} \tag{21}$$

and set $\mathbf{u}^{n+1/6} = \mathbf{u}(t^{n+1})$, $p^{n+1/6} = p(t^{n+1})$.

Next, compute $\mathbf{u}^{n+2/6}$ via the solution of

$$\begin{cases} \int_\Omega \frac{\partial \mathbf{u}}{\partial t} \cdot \mathbf{v}\,d\mathbf{x} + \int_\Omega (\mathbf{u}^{n+1/6} \cdot \nabla)\mathbf{u} \cdot \mathbf{v}\,d\mathbf{x} = 0, \quad \forall \mathbf{v} \in \mathbf{W}_0^{n+1,-}, \\ \quad \text{a.e. on } (t^n, t^{n+1}), \\ \mathbf{u}(t^n) = \mathbf{u}^{n+1/6}, \\ \mathbf{u}(t) \in (H^1(\Omega))^3, \mathbf{u}(t) = \mathbf{g}(t^{n+1}) \\ \quad \text{on } \Gamma_-^{n+1} \times (t^n, t^{n+1}), \end{cases} \tag{22}$$

and set $\mathbf{u}^{n+2/6} = \mathbf{u}(t^{n+1})$.

Then, compute $\mathbf{u}^{n+3/6}$ via the solution of

$$\begin{cases} \rho_f \int_\Omega \frac{\partial \mathbf{u}}{\partial t} \cdot \mathbf{v}\,d\mathbf{x} + \alpha \nu_f \int_\Omega \nabla \mathbf{u} : \nabla \mathbf{v}\,d\mathbf{x} = \mathbf{0}, \quad \forall \mathbf{v} \in (H_0^1(\Omega))^3, \\ \quad \text{a.e. on } (t^n, t^{n+1}), \\ \mathbf{u}(t^n) = \mathbf{u}^{n+2/6}, \\ \mathbf{u}(t) \in (H^1(\Omega))^3, \mathbf{u}(t) = \mathbf{g}(t^{n+1}) \\ \quad \text{on } \Gamma \times (t^n, t^{n+1}), \end{cases} \tag{23}$$

and set $\mathbf{u}^{n+3/6} = \mathbf{u}(t^{n+1})$.

Now predict the motion of the center of mass and the angular velocity of the particle via

$$\frac{d\mathbf{G}}{dt} = \mathbf{V}(t)/2, \tag{24}$$

$$\left(1 - \frac{\rho_f}{\rho_s}\right) M_p \frac{d\mathbf{V}}{dt} = \mathbf{F}^r/2, \tag{25}$$

$$\left(1 - \frac{\rho_f}{\rho_s}\right) \frac{d(\mathbf{I}_p \boldsymbol{\omega})}{dt} = \overrightarrow{\mathbf{G}\mathbf{x}_\mathbf{r}} \times \mathbf{F}_r/2, \tag{26}$$

$$\frac{d\mathbf{x}_i}{dt} = \mathbf{V}(t) + \boldsymbol{\omega}(t) \times \overrightarrow{\mathbf{G}(t)\mathbf{x}_i}, \quad \text{for } i = 1, 2, \tag{27}$$

$$\begin{aligned} &\mathbf{G}(t^n) = \mathbf{G}^n, \quad \mathbf{V}(t^n) = \mathbf{V}^n, \quad (\mathbf{I}_p \boldsymbol{\omega})(t^n) = (\mathbf{I}_p \boldsymbol{\omega})^n, \\ &\mathbf{x}_1(t^n) = \mathbf{x}_1^n, \quad \mathbf{x}_2(t^n) = \mathbf{x}_2^n, \end{aligned} \tag{28}$$

for $t^n < t < t^{n+1}$. Then set $\mathbf{G}^{n+4/6} = \mathbf{G}(t^{n+1})$, $\mathbf{V}^{n+4/6} = \mathbf{V}(t^{n+1})$, $(\mathbf{I}_p \boldsymbol{\omega})^{n+4/6} = (\mathbf{I}_p \boldsymbol{\omega})(t^{n+1})$, $\mathbf{x}_1^{n+4/6} = \mathbf{x}_1(t^{n+1})$, and $\mathbf{x}_2^{n+4/6} = \mathbf{x}_2(t^{n+1})$.

Using $\mathbf{G}^{n+4/6}$, $\mathbf{x}_1^{n+4/6}$ and $\mathbf{x}_2^{n+4/6}$ obtained in the above step, we enforce the rigid body motion in the region $B^{n+4/6}$ occupied by the particle

$$\begin{cases} \rho_f \int_\Omega \frac{\partial \mathbf{u}}{\partial t} \cdot \mathbf{v}\,d\mathbf{x} + \beta \nu_f \int_\Omega \nabla \mathbf{u} : \nabla \mathbf{v}\,d\mathbf{x} + \left(1 - \frac{\rho_f}{\rho_s}\right) M_p \frac{d\mathbf{V}}{dt} \cdot \mathbf{Y} \\ \quad + \left(1 - \frac{\rho_f}{\rho_s}\right) \frac{d(\mathbf{I}_p \boldsymbol{\omega})}{dt} \cdot \boldsymbol{\theta} = \left(1 - \frac{\rho_f}{\rho_s}\right) M_p \mathbf{g} \cdot \mathbf{Y} \\ \quad + \langle \boldsymbol{\lambda}, \mathbf{v} - \mathbf{Y} - \boldsymbol{\theta} \times \overrightarrow{\mathbf{G}^{n+4/6}\mathbf{x}} \rangle_{\Lambda^{n+4/6}}, \\ \forall \mathbf{v} \in (H_0^1(\Omega))^3, \mathbf{Y} \in \mathbb{R}^3, \boldsymbol{\theta} \in \mathbb{R}^3, \quad \text{a.e. on } (t^n, t^{n+1}), \\ \mathbf{u}(t^n) = \mathbf{u}^{n+3/6}, \\ \mathbf{u} \in (H^1(\Omega))^3, \mathbf{u}(t) = \mathbf{g}_0(t^{n+1}) \quad \text{on } \Gamma \times (t^n, t^{n+1}), \\ \boldsymbol{\lambda} \in \Lambda^{n+4/6}, \mathbf{Y} \in \mathbb{R}^3, \boldsymbol{\omega} \in \mathbb{R}^3, \end{cases} \tag{29}$$

$$\langle \boldsymbol{\mu}, \mathbf{u} - \mathbf{V} - \boldsymbol{\omega} \times \overrightarrow{\mathbf{G}^{n+4/6}\mathbf{x}} \rangle_{\Lambda^{n+4/6}} = 0, \quad \forall \boldsymbol{\mu} \in \Lambda^{n+4/6}, \tag{30}$$

and set $\mathbf{u}^{n+1} = \mathbf{u}(t^{n+1})$, $\mathbf{V}^{n+5/6} = V(t^{n+1})$, $(\mathbf{I}_p \boldsymbol{\omega})^{n+5/6} = (\mathbf{I}_p\ \boldsymbol{\omega})(t^{n+1})$.

Correct the motion of the center of mass and the angular velocity of the particle via

$$\frac{d\mathbf{G}}{dt} = \mathbf{V}(t)/2, \tag{31}$$

$$\left(1 - \frac{\rho_f}{\rho_s}\right) M_p \frac{d\mathbf{V}}{dt} = \mathbf{F}^r/2, \tag{32}$$

$$\left(1 - \frac{\rho_f}{\rho_s}\right) \frac{d(\mathbf{I}_p \boldsymbol{\omega})}{dt} = \overrightarrow{\mathbf{G}x_r} \times \mathbf{F}_r/2, \tag{33}$$

$$\frac{d\mathbf{x}_i}{dt} = \mathbf{V}(t) + \boldsymbol{\omega}(t) \times \overrightarrow{\mathbf{G}(t)\mathbf{x}_i}, \quad \text{for } i = 1, 2, \tag{34}$$

$$\begin{aligned} &\mathbf{G}(t^n) = \mathbf{G}^{n+4/6}, \quad \mathbf{V}(t^n) = \mathbf{V}^{n+5/6}, \\ &(\mathbf{I}_p \boldsymbol{\omega})(t^n) = (\mathbf{I}_p \boldsymbol{\omega})^{n+5/6}, \\ &\mathbf{x}_1(t^n) = \mathbf{x}_1^{n+4/6}, \quad \mathbf{x}_2(t^n) = \mathbf{x}_2^{n+4/6}, \end{aligned} \tag{35}$$

for $t^n < t < t^{n+1}$. Then set $\mathbf{G}^{n+1} = G(t^{n+1})$, $\mathbf{V}^{n+1} = \mathbf{V}(t^{n+1})$, $(\mathbf{I}_p \boldsymbol{\omega})^{n+1} = (\mathbf{I}_p \boldsymbol{\omega})(t^{n+1})$, $\mathbf{x}_1^{n+1} = \mathbf{x}_1(t^{n+1})$, and $\mathbf{x}_2^{n+1} = \mathbf{x}_2(t^{n+1})$.

In (20)–(32), $\Gamma_-^{n+1} = \{\mathbf{x} \mid \mathbf{x} \in \Gamma, \mathbf{g}_0(t^{n+1})(\mathbf{x}) \cdot \mathbf{n}(\mathbf{x}) < 0\}$ and $\mathbf{W}_0^{n+1,-} = \{\mathbf{v} \mid \mathbf{v} \in (H^1(\Omega))^3, \mathbf{v} = \mathbf{0} \text{ on } \Gamma_-^{n+1}\}$, $\Lambda^{n+4/6} = (H^1(B^{n+4/6}))^3$, $B^{n+4/6}$ is the region occupied by the particle B according to $\mathbf{G}^{n+4/6}$, $\mathbf{x}_1^{n+4/6}$ and $\mathbf{x}_2^{n+4/6}$, and $\alpha+\beta = 1$. In the numerical simulation, we usually choose $\alpha = 1$ and $\beta = 0$.

3.2. Space discretization

We assume that $\Omega \subset \mathbb{R}^3$ and is a rectangular parallelepiped. Concerning the *finite element approximation* of problem (12)–(19), we have

$$\mathbf{W}_h = \{\mathbf{v}_h \mid \mathbf{v}_h \in (C^0(\overline{\Omega}))^3, \mathbf{v}_h|_T \in (P_1)^3, \quad \forall T \in \mathscr{T}_h\}, \tag{36}$$

$$\mathbf{W}_{0h} = \{\mathbf{v}_h \mid \mathbf{v}_h \in \mathbf{W}_h, \mathbf{v}_h = \mathbf{0} \quad \text{on } \Gamma\}, \tag{37}$$

$$L_h^2 = \{q_h \mid q_h \in C^0(\overline{\Omega}), q_h|_T \in P_1, \quad \forall T \in \mathscr{T}_{2h}\},$$
$$L_{0h}^2 = \left\{q_h \mid q_h \in L_h^2, \int_\Omega q_h \,\mathrm{d}\mathbf{x} = 0\right\} \tag{38}$$

where $\mathscr{T}_h$ is a tetrahedrization of Ω, $\mathscr{T}_{2h}$ is twice coarser than $\mathscr{T}_h$, and P_1 is the space of the polynomials in three variables of degree $\leqslant 1$. A finite dimensional space approximating $\Lambda(t)$ is as follows: let $\{\boldsymbol{\xi}_i\}_{i=1}^N$ be a set of points from $\overline{B(t)}$ which cover $\overline{B(t)}$ (uniformly, for example); we define then

$$\Lambda_h(t) = \left\{\boldsymbol{\mu}_h \mid \boldsymbol{\mu}_h = \sum_{i=1}^N \boldsymbol{\mu}_i \delta(\mathbf{x} - \boldsymbol{\xi}_i), \boldsymbol{\mu}_i \in \mathbb{R}^3, \right.$$
$$\left. \forall i = 1, \ldots, N\right\}, \tag{39}$$

where $\delta(\cdot)$ is the Dirac measure at $\mathbf{x} = \mathbf{0}$. Then we shall use $\langle \cdot, \cdot \rangle_h$ defined by

$$\langle \boldsymbol{\mu}_h, \mathbf{v}_h \rangle_h = \sum_{i=1}^N \boldsymbol{\mu}_i \cdot \mathbf{v}_h(\boldsymbol{\xi}_i), \forall \boldsymbol{\mu}_h \in \Lambda_h(t), \mathbf{v}_h \in \mathbf{W}_h. \tag{40}$$

A typical choice of points for defining (39) is to take the grid points of the velocity mesh internal to the particle B and whose distance to the boundary of B is greater than, e.g. $h/2$, and to complete with selected points from the boundary of $B(t)$ (e.g., see Fig. 2 for an example of selected points on the boundary of $B(t)$).

Using the above finite dimensional spaces and the backward Euler's method for most of the subproblems

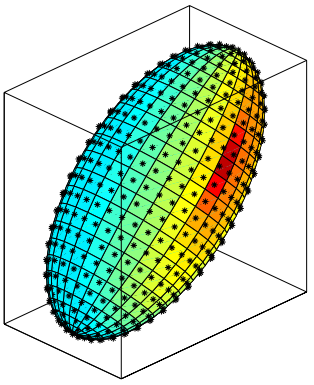

Fig. 2. An example of selected points on the boundary of the particle.

in scheme (20)–(35), we obtain the following scheme after dropping some of the subscripts h (similar ones are discussed in [9,10,16–18]):

$$\mathbf{u}^0 = \tilde{\mathbf{u}}_0, \quad \mathbf{G}^0 = \mathbf{G}_0, \quad \mathbf{V}^0 = \mathbf{V}_0, \quad \boldsymbol{\omega}^0 = \boldsymbol{\omega}_0,$$
$$\mathbf{x}_1^0 = \mathbf{x}_{1,0}, \quad \mathbf{x}_2^0 = \mathbf{x}_{2,0} \text{ given;} \tag{41}$$

for $n \geqslant 0$, $\mathbf{u}^n (\simeq \mathbf{u}(t^n))$, $\mathbf{G}^n$, $\mathbf{V}^n$, $\boldsymbol{\omega}^n$, $\mathbf{x}_1^n$ and $\mathbf{x}_2^n$ *being known, we compute* $\mathbf{u}^{n+1/6}$, $p^{n+1/6}$ via the solution of

$$\begin{cases} \rho_f \int_\Omega \frac{\mathbf{u}^{n+1/6} - \mathbf{u}^n}{\Delta t} \cdot \mathbf{v} \,\mathrm{d}\mathbf{x} - \int_\Omega p^{n+1/6} \nabla \cdot \mathbf{v} \,\mathrm{d}\mathbf{x} = 0, \quad \forall \mathbf{v} \in \mathbf{W}_{0h}, \\ \int_\Omega q \nabla \cdot \mathbf{u}^{n+1/6} \,\mathrm{d}\mathbf{x} = 0, \quad \forall q \in L_h^2, \\ \mathbf{u}^{n+1/6} \in \mathbf{W}_h, \mathbf{u}^{n+1/6} = \mathbf{g}_{0h}^{n+1} \quad \text{on } \Gamma, p^{n+1/6} \in L_{0h}^2. \end{cases} \tag{42}$$

Next, compute $\mathbf{u}^{n+2/6}$ via the solution of

$$\begin{cases} \int_\Omega \frac{\partial \mathbf{u}}{\partial t} \cdot \mathbf{v} \,\mathrm{d}\mathbf{x} + \int_\Omega (\mathbf{u}^{n+1/6} \cdot \nabla)\mathbf{u} \cdot \mathbf{v} \,\mathrm{d}\mathbf{x} = 0, \\ \forall \mathbf{v} \in \mathbf{W}_{0h}^{n+1,-}, \quad \text{a.e. on } (t^n, t^{n+1}), \\ \mathbf{u}(t^n) = \mathbf{u}^{n+1/6}, \\ \mathbf{u}(t) \in \mathbf{W}_h, \mathbf{u}(t) = \mathbf{g}_{0h}^{n+1} \quad \text{on } \Gamma_-^{n+1} \times (t^n, t^{n+1}), \end{cases} \tag{43}$$

and set $\mathbf{u}^{n+2/6} = \mathbf{u}(t^{n+1})$.

Then, compute $\mathbf{u}^{n+3/6}$ via the solution of

$$\begin{cases} \rho_f \int_\Omega \frac{\mathbf{u}^{n+3/6} - \mathbf{u}^{n+2/6}}{\Delta t} \cdot \mathbf{v} \,\mathrm{d}\mathbf{x} + \alpha \nu_f \int_\Omega \nabla \mathbf{u}^{n+3/6} : \nabla \mathbf{v} \,\mathrm{d}\mathbf{x} = 0, \\ \forall \mathbf{v} \in \mathbf{W}_{0h}; \mathbf{u}^{n+3/6} \in \mathbf{W}_h, \mathbf{u}^{n+3/6} = \mathbf{g}_{0h}^{n+1} \quad \text{on } \Gamma. \end{cases} \tag{44}$$

Now predict the motion of the center of mass and the angular velocity of the particle via

$$\frac{\mathrm{d}\mathbf{G}}{\mathrm{d}t} = \mathbf{V}(t)/2, \tag{45}$$

$$\left(1 - \frac{\rho_f}{\rho_s}\right) M_p \frac{\mathrm{d}\mathbf{V}}{\mathrm{d}t} = \mathbf{F}^r/2, \tag{46}$$

$$\left(1 - \frac{\rho_f}{\rho_s}\right) \frac{\mathrm{d}(\mathbf{I}_p \boldsymbol{\omega})}{\mathrm{d}t} = \vec{\mathbf{G}x}_r \times \mathbf{F}_r/2, \tag{47}$$

$$\frac{\mathrm{d}\mathbf{x}_i}{\mathrm{d}t} = \mathbf{V}(t) + \boldsymbol{\omega}(t) \times \overrightarrow{\mathbf{G}(t)\mathbf{x}_i}, \quad \text{for } i = 1, 2, \tag{48}$$

$$\mathbf{G}(t^n) = \mathbf{G}^n, \mathbf{V}(t^n) = \mathbf{V}^n, (\mathbf{I}_p \boldsymbol{\omega})(t^n) = (\mathbf{I}_p \boldsymbol{\omega})^n,$$
$$\mathbf{x}_1(t^n) = \mathbf{x}_1^n, \ \mathbf{x}_2(t^n) = \mathbf{x}_2^n, \tag{49}$$

for $t^n < t < t^{n+1}$.

Then set $\mathbf{G}^{n+4/6} = \mathbf{G}(t^{n+1})$, $\mathbf{V}^{n+4/6} = V(t^{n+1})$, $(\mathbf{I}_p \boldsymbol{\omega})^{n+4/6} = (\mathbf{I}_p \boldsymbol{\omega})(t^{n+1})$, $\mathbf{x}_1^{n+4/6} = \mathbf{x}_1(t^{n+1})$, and $\mathbf{x}_2^{n+4/6} = \mathbf{x}_2(t^{n+1})$.

With the center $\mathbf{G}^{n+4/6}$, $\mathbf{x}_1^{n+4/6}$ and $\mathbf{x}_2^{n+4/6}$ obtained at the above step, we enforce the rigid body motion in the region $B(t^{n+4/6})$ occupied by the particle

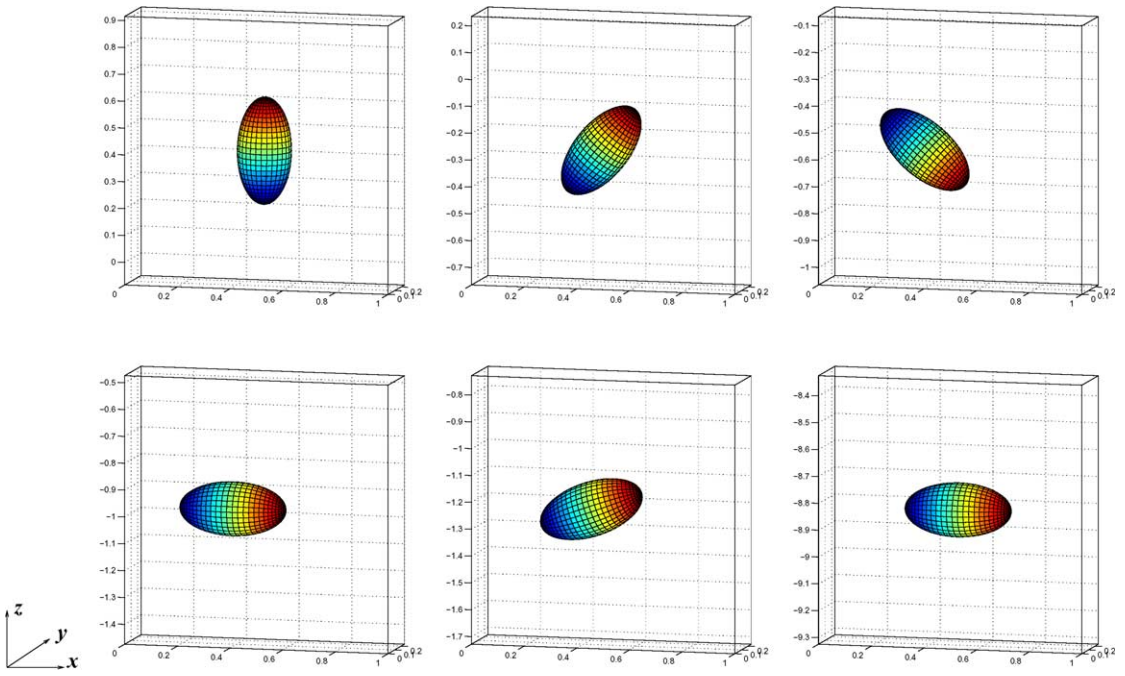

Fig. 3. Position of the ellipsoid at $t = 0.2$, 0.35, 0.45, 0.6, 0.7 and 4 (from left to right and from top to bottom).

$$\begin{cases} \rho_f \int_\Omega \frac{\mathbf{u}^{n+1}-\mathbf{u}^{n+4/6}}{\Delta t}\cdot\mathbf{v}\,d\mathbf{x} + \beta\nu_f\int_\Omega \nabla\mathbf{u}^{n+1}:\nabla\mathbf{v}\,d\mathbf{x} \\ \quad +\left(1-\frac{\rho_f}{\rho_s}\right)M_p\frac{\mathbf{V}^{n+5/6}-\mathbf{V}^{n+4/6}}{\Delta t}\cdot\mathbf{Y} \\ \quad +\left(1-\frac{\rho_f}{\rho_s}\right)\frac{(\mathbf{I}_p\boldsymbol{\omega})^{n+5/6}-(\mathbf{I}_p\boldsymbol{\omega})^{n+4/6}}{\Delta t}\cdot\boldsymbol{\theta} \\ \quad = \left(1-\frac{\rho_f}{\rho_s}\right)M_p\mathbf{g}\cdot\mathbf{Y} + \langle\boldsymbol{\lambda}^{n+4/6}, \mathbf{v}-\mathbf{Y}-\boldsymbol{\theta}\times\overrightarrow{\mathbf{G}^{n+4/6}}\mathbf{x}\rangle_h, \\ \forall\mathbf{v}\in\mathbf{W}_{0h},\mathbf{Y}\in\mathbb{R}^3,\boldsymbol{\theta}\in\mathbb{R}^3; \\ \mathbf{u}^{n+1}\in\mathbf{W}_h, \mathbf{u}^{n+1}=\mathbf{g}_{0h}^{n+1} \quad \text{on } \Gamma, \boldsymbol{\lambda}^{n+4/6}\in\Lambda_h^{n+4/6}, \\ \mathbf{V}^{n+5/6}\in\mathbb{R}^3, \boldsymbol{\omega}^{n+5/6}\in\mathbb{R}^3, \end{cases} \tag{50}$$

$$\langle\boldsymbol{\mu}, \mathbf{u}^{n+1}-\mathbf{V}^{n+5/6}-\boldsymbol{\omega}^{n+5/6}\times\overrightarrow{\mathbf{G}_j^{n+4/6}}\mathbf{x}\rangle_h = 0, \quad \forall\boldsymbol{\mu}\in\Lambda_h^{n+4/6}. \tag{51}$$

Correct the motion of the center of mass and the angular velocity of the particle via

$$\frac{d\mathbf{G}}{dt} = \mathbf{V}(t)/2, \tag{52}$$

$$\left(1-\frac{\rho_f}{\rho_s}\right)M_p\frac{d\mathbf{V}}{dt} = \mathbf{F}^r/2, \tag{53}$$

$$\left(1-\frac{\rho_f}{\rho_s}\right)\frac{d(\mathbf{I}_p\boldsymbol{\omega})}{dt} = \vec{\mathbf{G}}x_r\times\mathbf{F}_r/2, \tag{54}$$

$$\frac{d\mathbf{x}_i}{dt} = \mathbf{V}(t)+\boldsymbol{\omega}(t)\times\overrightarrow{\mathbf{G}(t)}\mathbf{x}_i, \quad \text{for } i=1,2, \tag{55}$$

$$\mathbf{G}(t^n)=\mathbf{G}^{n+4/6}, \quad \mathbf{V}(t^n)=\mathbf{V}^{n+5/6}, \quad (\mathbf{I}_p\boldsymbol{\omega})(t^n)=(\mathbf{I}_p\boldsymbol{\omega})^{n+5/6},$$

$$\mathbf{x}_1(t^n)=\mathbf{x}_1^{n+4/6}, \quad \mathbf{x}_2(t^n)=\mathbf{x}_2^{n+4/6}, \tag{56}$$

for $t^n < t < t^{n+1}$. Then set $\mathbf{G}^{n+1} = G(t^{n+1})$, $\mathbf{V}^{n+1} = \mathbf{V}(t^{n+1})$, $(\mathbf{I}_p\boldsymbol{\omega})^{n+1} = (\mathbf{I}_p\boldsymbol{\omega})(t^{n+1})$, $\mathbf{x}_1^{n+1} = \mathbf{x}_1(t^{n+1})$, and $\mathbf{x}_2^{n+1} = \mathbf{x}_2(t^{n+1})$.

In (41)–(56), $\Gamma_-^{n+1} = \{\mathbf{x} \mid \mathbf{x}\in\Gamma,\ \mathbf{g}_{0h}^{n+1}(\mathbf{x})\cdot\mathbf{n}(\mathbf{x})<0\}$ and $\mathbf{W}_{0h}^{n+1,-} = \{\mathbf{v} \mid \mathbf{v}\in\mathbf{W}_h, \mathbf{v}=\mathbf{0} \text{ on } \Gamma_-^{n+1}\}$, $\Lambda_h^{n+s} = \Lambda_h(t^{n+s})$, $\mathbf{g}_{0h}^{n+1}$ is an approximation of $\mathbf{g}_0^{n+1}$ belonging to

$$\gamma\mathbf{W}_h = \{\mathbf{z}_h \mid \mathbf{z}_h\in(C^0(\Gamma))^3, \quad \mathbf{z}_h=\tilde{\mathbf{z}}_h|_\Gamma \text{ with } \tilde{\mathbf{z}}_h\in\mathbf{W}_h\}$$

and verifying $\int_\Gamma \mathbf{g}_{0h}^{n+1}\cdot\mathbf{n}\,d\Gamma = 0$.

Remark 2. When applying the backward Euler method to all the subproblems in cheme (20)–(35), we obtain a fractional step scheme à la Marchuk–Yanenko [30], which is only first order accurate but its low-order accuracy is compensated by good stability and robustness properties. The preliminary numerical results obtained via the variant of the above scheme (the one without the correction step for the particle motion) were presented in [31]. The above algorithm (41)–(56) gives us better convergent result which has been presented in Section 4. The rate of convergence, when using Taylor–Hood finite element approximation, has been investigated in [13] for a circular particle in Stokes flow, the

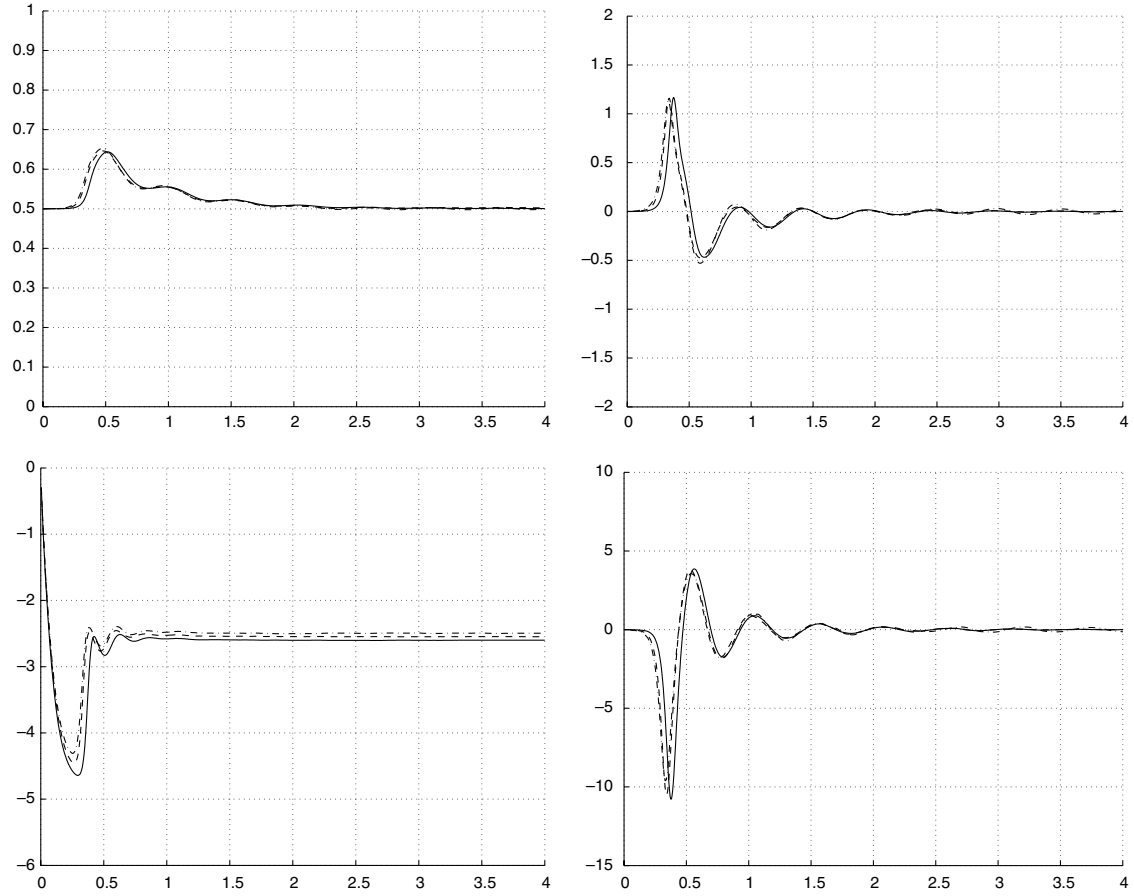

Fig. 4. Histories of the x-coordinate of the mass center (upper left), the horizontal velocity of the mass center (upper right), the vertical velocity of the mass center (lower left) and the angular velocity with respect to the y-axis (lower right) ($h_v = 1/80$ and $\Delta t = 0.001$, dashed-dotted lines; $h_v = 1/112$ and $\Delta t = 0.0005$, dashed lines; $h_v = 1/160$ and $\Delta t = 0.0005$, solid lines).

error orders in L^2-norm for velocity and pressure are a bit beyond 3 and 2, respectively.

3.3. On the solution of subproblems (42)–(49), and (50) and (51)

The degenerated quasi-Stokes problem (42) is solved by an Uzawa/preconditioned conjugate gradient algorithm as in [32], where the discrete elliptic problems used for preconditioning are solved by a matrix-free fast solver from FISHPAK due to Adams et al. in [33]. The stopping criterion for the preconditioned conjugate gradient algorithm is $\|\mathbf{r}^k\|/\|\mathbf{r}^0\| \leqslant \epsilon$ where $\mathbf{r}^k$ is the residue at the kth iteration. It typically takes about 10 iterations in the simulation with $\epsilon = 10^{-5}$. The advection problem (43) for the velocity field is solved by a wave-like equation method as in [34,35]. Problem (44) is a classical discrete elliptic problem which can be solved by the above matrix-free fast solver.

Systems (45)–(49) and (52)–(56) are systems of ordinary differential equations thanks to operator splitting. For its solution one can choose a time step smaller than Δt, (i.e., we can divide Δt into smaller steps) to predict the translation velocity of the center of mass, the angular velocity of the particle, the position of the center of mass and the regions occupied by each particle so that the repulsion forces can be effective to prevent particle-particle and particle-wall overlapping. At each sub-cycling time step, keeping the distance constant between points $\mathbf{x}_1$ and $\mathbf{x}_2$ in each particle is important since we are dealing with rigid particles. To satisfy the above constraint we have applied the following approach:

- Translate $\mathbf{x}_1$ and $\mathbf{x}_2$ according to the new position of the mass center at each sub-cycling time step.

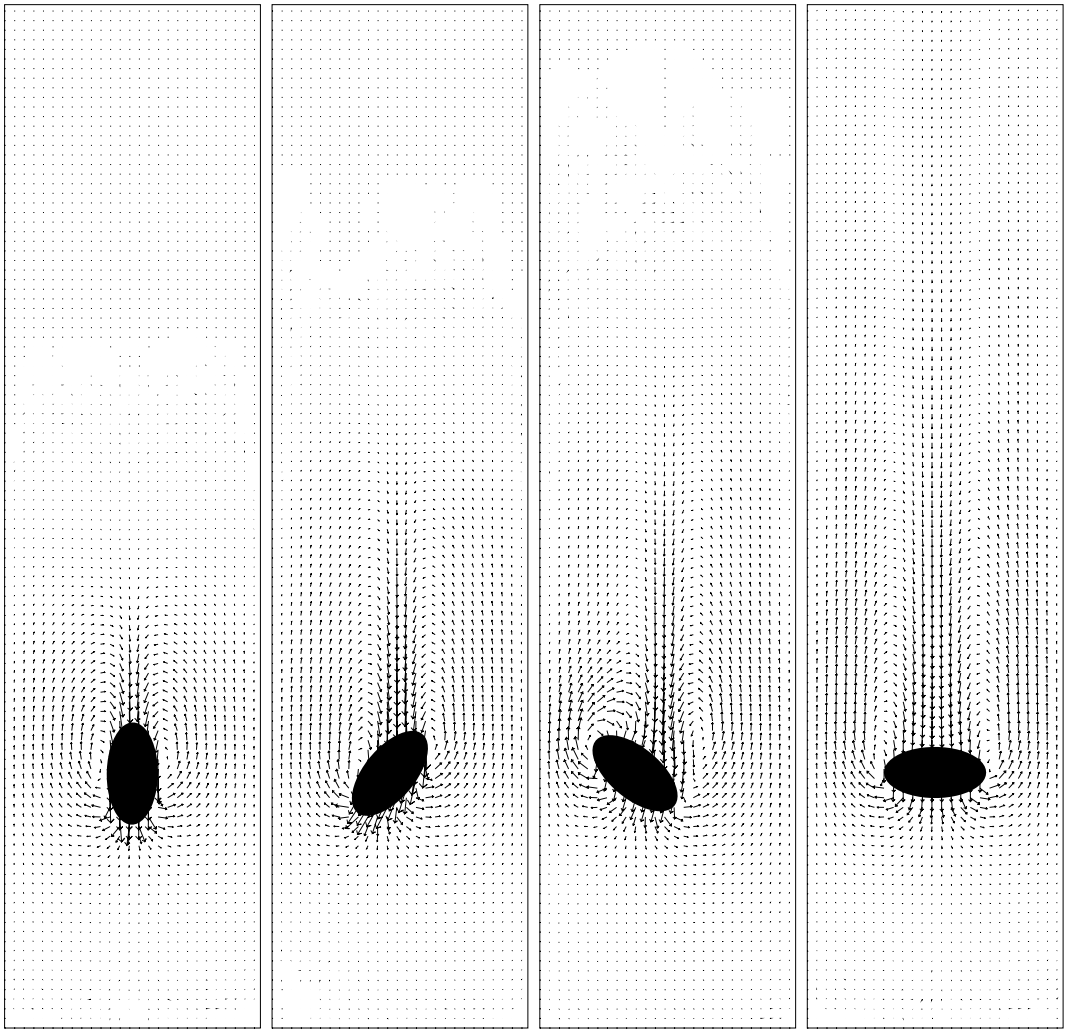

Fig. 5. Velocity field at $t = 0.2$, 0.35, 0.45 and 4 on the plane passing through the mass center of the left ellipsoid (from left to right).

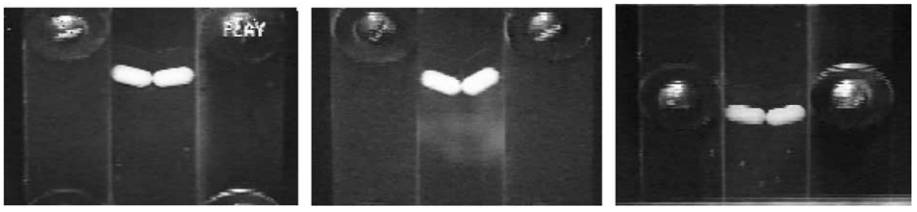

Fig. 6. Snapshots of a period of the motion of two cylinders with round ends sedimenting in a narrow channel filled with a Newtonian fluid.

- Rotate $\mathbf{G}\,x_1$ and $\mathbf{G}\,x_2$, the relative positions of $\mathbf{x}_1$ and $\mathbf{x}_2$ to the center of mass $\mathbf{G}$, by the following Crank–Nicolson scheme (a Runge–Kutta scheme of order 2, in fact):

$$\frac{\mathbf{G}\mathbf{x}_i^{\text{new}} - \mathbf{G}\mathbf{x}_i^{\text{old}}}{\tau} = \boldsymbol{\omega} \times \frac{\mathbf{G}\mathbf{x}_i^{\text{new}} + \mathbf{G}\mathbf{x}_i^{\text{old}}}{2} \tag{57}$$

for $i = 1,2$ with τ as a sub-cycling time step. By (57), we have $|\mathbf{G}\mathbf{x}_i^{\text{new}}|^2 = |\mathbf{G}\mathbf{x}_i^{\text{old}}|^2$ for $i = 1,2$ and

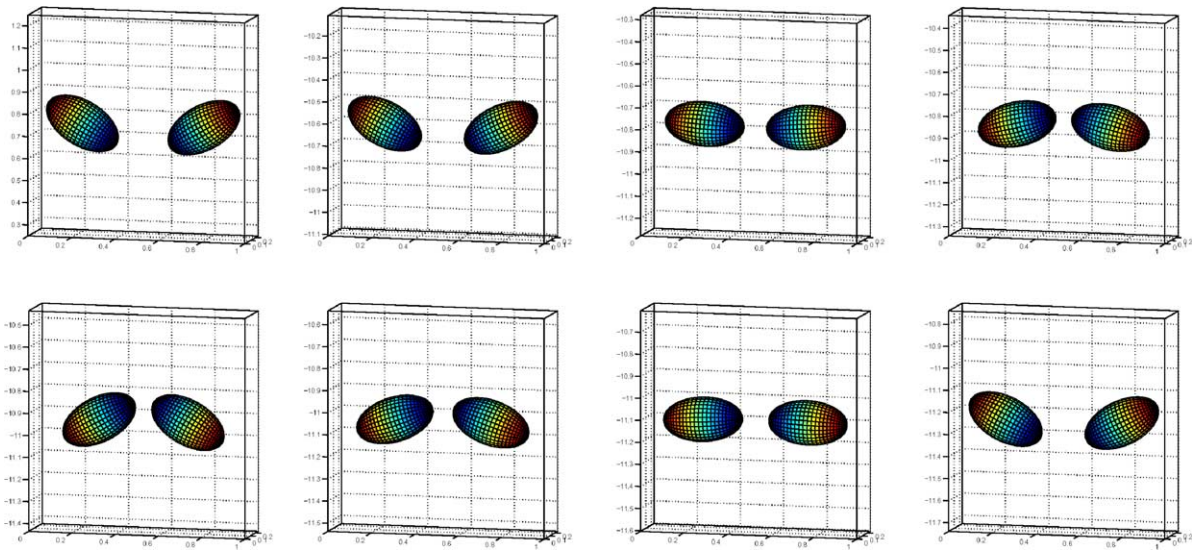

Fig. 7. Position of ellipsoids at $t = 0$, 7.058, 7.16, 7.20, 7.26, 7.32, 7.36 and 7.448 (from left to right and from top to bottom). The last seven positions are taken from one period of motion.

$|\mathbf{G}\mathbf{x}_2^{\text{new}} - \mathbf{G}\mathbf{x}_1^{\text{new}}|^2 = |\mathbf{G}\mathbf{x}_2^{\text{old}} - \mathbf{G}\mathbf{x}_1^{\text{old}}|^2$ (i.e., scheme (57) is distance and in fact shape preserving).

Remark 3. In order to activate the short range repulsion force, we have to find the shortest distance between two ellipsoids. Unlike the cases for spheres, it is not trivial to locate the point from each surface of the ellipsoid where the distance is the shortest between two ellipsoids. There is no explicit formula for such distance. In practice, we first choose a set of points from the surface of each ellipsoid. Then we find the point among the chosen points from each surface at which the distance is the shortest. We repeat this (kind of relaxation) process in the neighborhood of the newly located point on each surface of ellipsoid until convergence, usually obtained in very few iterations.

For the shortest distance between the wall and ellipsoid, there exists an explicit formula. To check whether two ellipsoids overlap each other, there exists an algorithm used by people working on computer graphics and in robotics (e.g., see, [36]).

The rigid body motion is enforced in $B(t^{n+4/6})$, via Eq. (51). At the same time those hydrodynamical forces and gravity acting on the particles are also taken into account in order to update the translation and angular velocities of the particles. To solve (50) and (51), we use a conjugate gradient algorithm as discussed in [9]. Since we take $\beta = 0$ in (50) for the simulation, we actually do not need to solve any non-trivial linear systems for the velocity field; this saves a lot of computing time. To get the angular velocity $\boldsymbol{\omega}^{n+1}$, computed via

$$\boldsymbol{\omega}^{n+1} = (\mathbf{I}_p^{n+4/6})^{-1}(\mathbf{I}_p\boldsymbol{\omega})^{n+1}, \tag{58}$$

we need to have $\mathbf{I}_p^{n+4/6}$, the inertia of the particle $B(t^{n+4/6})$. We first compute the inertia $\mathbf{I}_0$ in the coordinate system attached to the particle. Then via the center of mass $\mathbf{G}^{n+4/6}$ and points $\mathbf{x}_1^{n+4/6}$ and $\mathbf{x}_2^{n+4/6}$, we have the rotation transformation $\mathbf{Q}$ ($QQ^T = \mathbf{Q}^T\mathbf{Q} = \mathbf{I}_d$, det$\mathbf{Q}$=1) which transforms vectors expressed in the particle frame to vectors in the flow domain coordinate system and $\mathbf{I}_p^{n+s} = \mathbf{Q}\mathbf{I}_0\mathbf{Q}^T$. Actually in order to update matrix $\mathbf{Q}$ we can also use *quaternion* techniques, as shown, in the review paper [37].

4. Numerical experiments

4.1. Settling of one ellipsoid

In the first test case, we consider the simulation of the motion of an ellipsoid settling in a narrow channel of infinite length filled with a Newtonian fluid. The computational domain is $\Omega = (0,1) \times (0, 0.25) \times (0,4)$ initially, then it moves down with the center of the ellipsoid (see, e.g., [2] for adjusting the computational domain according to the position of the particle). The fluid density is $\rho_f = 1$ and the fluid viscosity is $\nu_f = 0.01$. The flow field initial condition is $\mathbf{u} = \mathbf{0}$. The density of the ellipsoid is $\rho_s = 1.1$. The three semi-axes of the ellipsoid are 0.2, 0.1 and 0.1. Initially its longest axis is in the vertical direction. The initial position of the mass center is at $(0.5, 0.125, 1)$. The initial translation and angular velocities of the ellipsoid are $\mathbf{0}$. To check the conver-

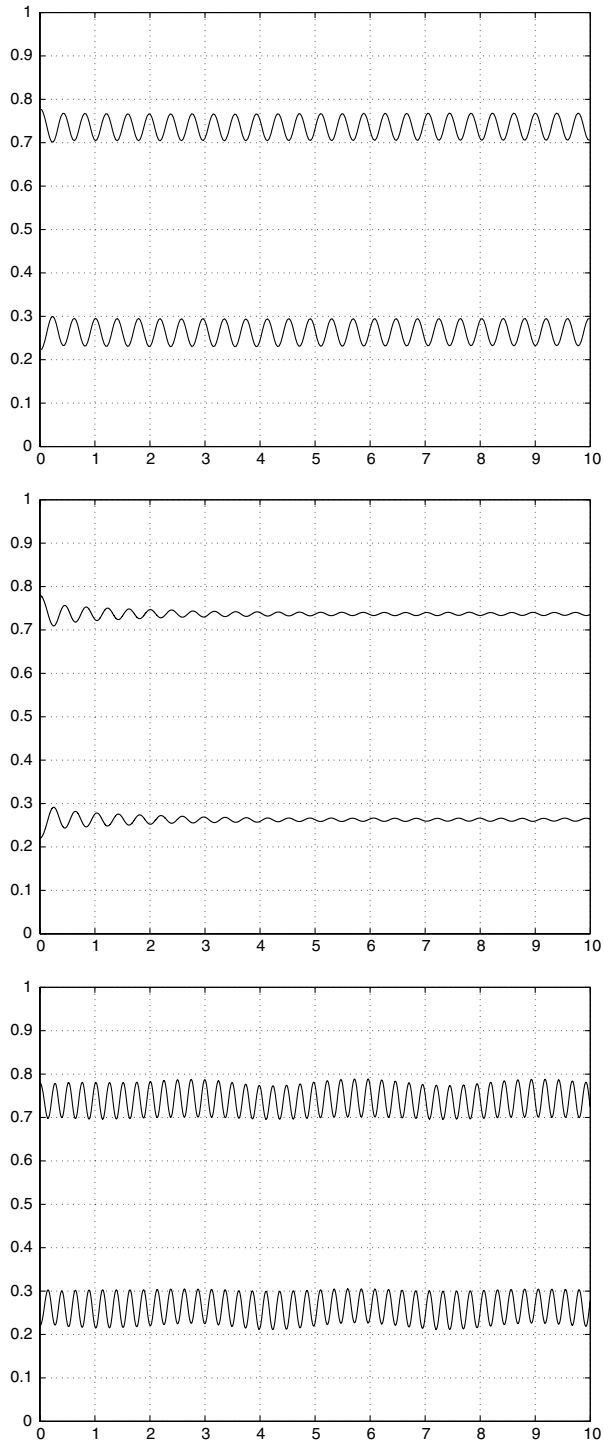

Fig. 8. Histories of the x-coordinates of the mass centers of two ellipsoids of long axis 0.36 (top), those of long axis 0.32 (middle) and those of the density 1.25 (bottom).

gence, we have chosen the following three pairs of the mesh size of the velocity field and the time step: $\{h_v,\Delta t\} = \{1/80, 0.001\}$, $\{1/112, 0.0005\}$ and $\{1/$

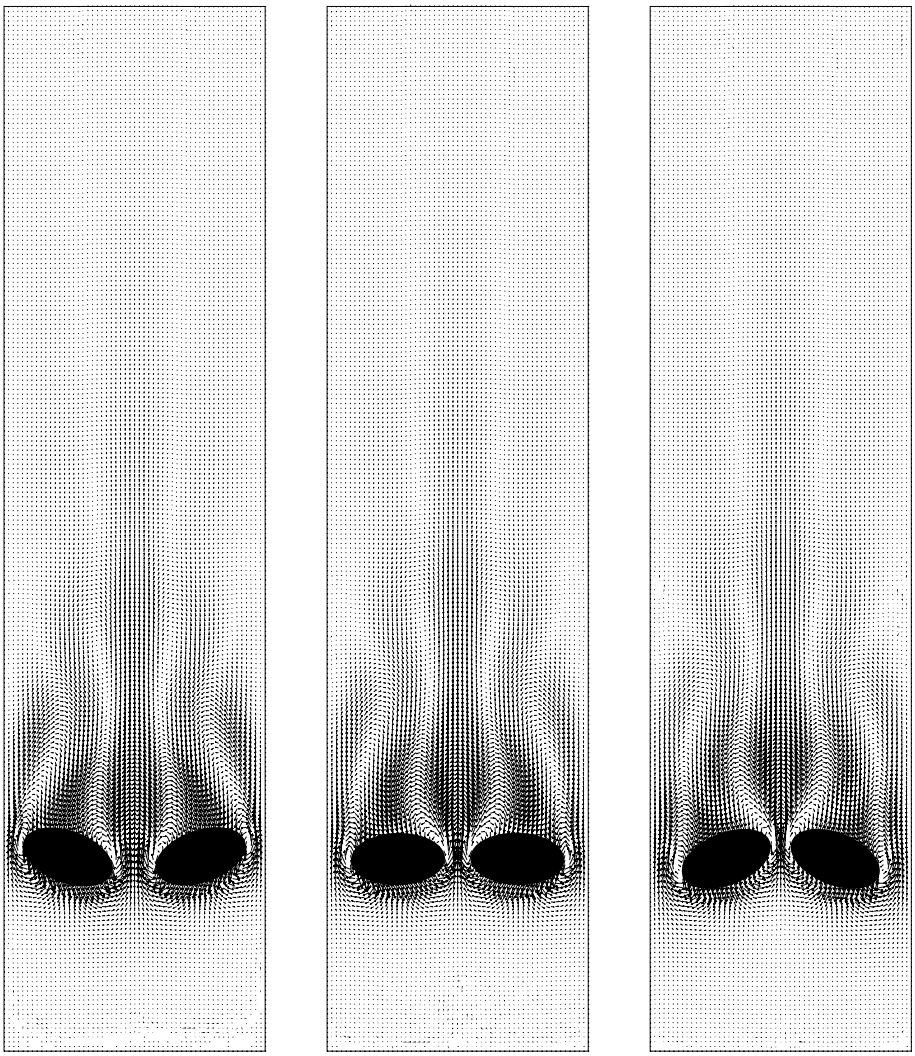

Fig. 9. Velocity field at $t = 4$, 6 and 8 on the plane passing through the mass center of the left ellipsoid (from left to right).

160, 0.0005}. The mesh size of the pressure is always $h_p = 2h_v$.

The snapshots of the ellipsoid position for $\{h_v,\Delta t\}=\{1/160, 0.0005\}$ at different times in the channel are shown in Fig. 3. The computation was performed in a moving frame of reference, so the ellipsoid appears not moving downward. The histories of the horizontal position, horizontal and vertical velocities of the mass center and the angular velocity with respect to the y-axis are shown in Fig. 4. We have obtained a good convergent result. The movement of the ellipsoid is very fast at the beginning when it moves toward the side wall after releasing from its initial position. Later on the oscillation has been damped out (see Fig. 4). As expected, the ellipsoid turns its broadside perpendicular to the stream main direction and the mass center moves back to the central axis of the channel. The velocity field projected to the xy-plane passing through the mass center are shown in Fig. 5 for $h_v = 1/160$ and $\Delta t = 0.0005$.

For $h_v = 1/160$ and $\Delta t = 0.0005$, the averaged particle speed when the ellipsoid reaches stable position is about 2.6 (the maximal speed is about 4.65) so the averaged particle Reynolds number with the longest axis as characteristic length is 104. The number of nodes for the velocity field is 546,021 (resp., 1,471,373 and 4,231,241) for $h_v = 1/80$ (resp., 1/112 and 1/160). The memory used in the simulation is about 68 Mb (resp., 182 and 523 Mb) for $h_v = 1/80$ (resp., 1/112 and 1/160). The simulation takes about 5 s (resp., 14 and 46 s) per time step for $\{h_v,\Delta t\} = \{1/80, 0.001\}$ (resp., {1/

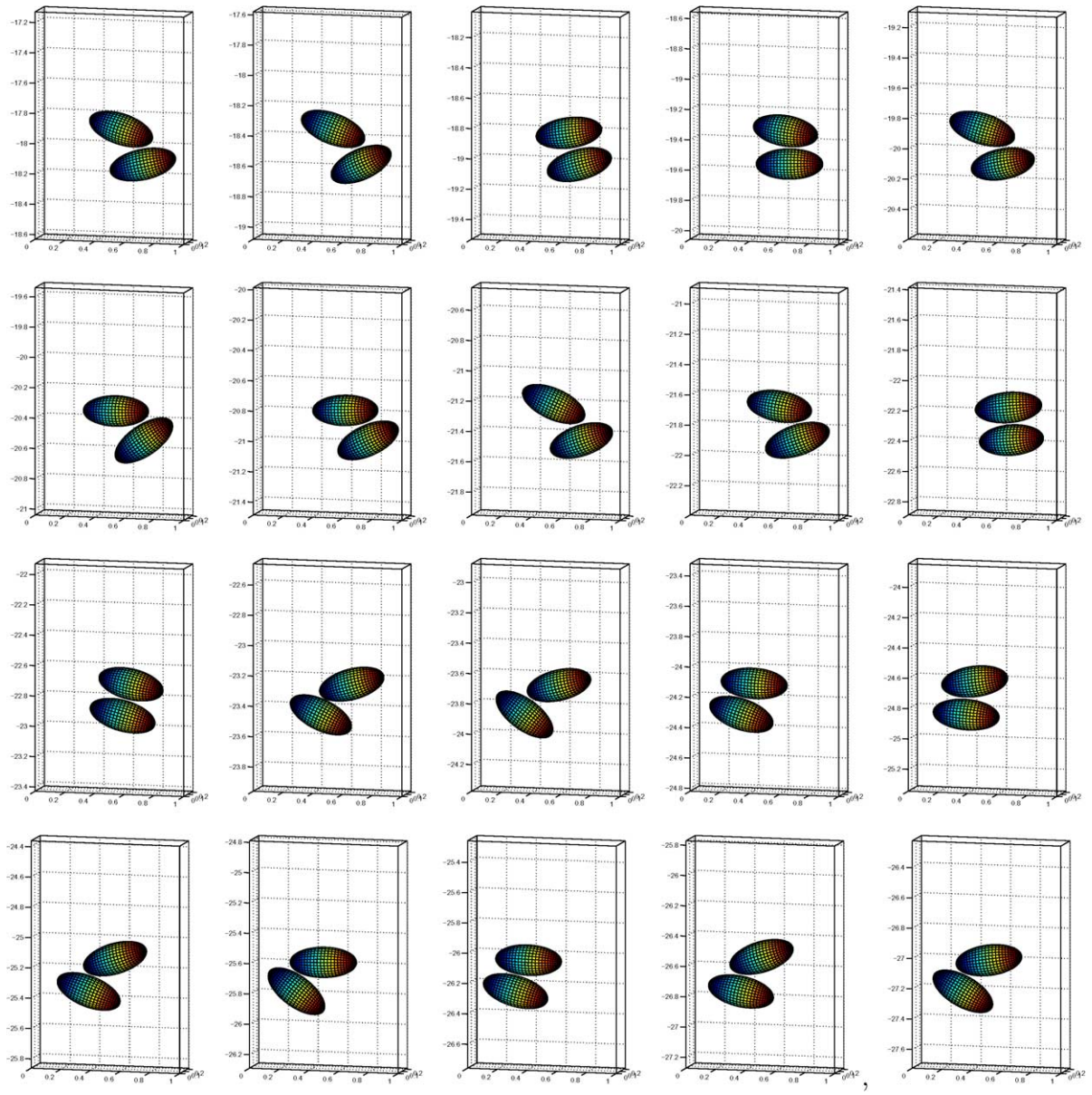

Fig. 10. Position of ellipsoids of long semi-axis 0.22 at t = 4.0, 4.1, 4.2, 4.3, 4.4, 4.5, 4.6, 4.7, 4.8, 4.9, 5.0, 5.1, 5.2, 5.3, 5.4, 5.5, 5.6, 5.7, 5.8, and 5.9 (from left to right and from top to bottom).

112, 0.0005} and {1/160, 0.0005}) on a Linux based PC with 2.2 GHz AMD Opteron CPU.

Remark 4. Due to the symmetry, there are two directions for a ellipsoid to settle after releasing from the initial position located at the central axis of the channel considered in this test case: to the left or to the right from the central axis. For $(h_v, \Delta t) = \{1/160, 0.0005\}$ the ellipsoid moves to the left and for the other two pairs of parameters, it moves to the right. In order to compare the results, the results for $(h_v,\Delta t) = \{1/160, 0.0005\}$ have been converted first and then plotted as shown in Fig. 4.

4.2. Two ellipsoids sedimenting side-by-side

It had been observed experimentally by Joseph et al. that when two cylinders with round ends sediment in a narrow channel filled with a Newtonian fluid, they can sediment side-by-side and interact each other periodi-

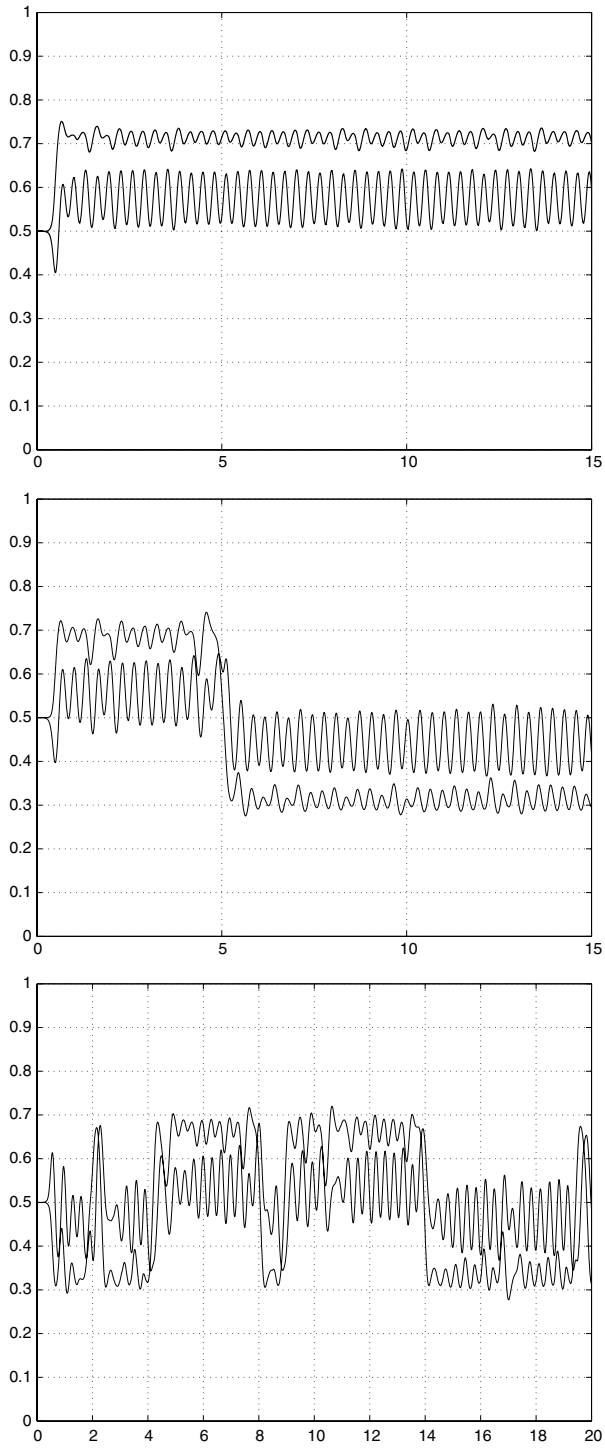

Fig. 11. Histories of the x-coordinates of the mass centers of two ellipsoids of semi-axis 0.21 (top), those of long semi-axis 0.22 (middle) and those of long semi-axis 0.23 (bottom).

cally as shown in Fig. 6. To reproduce similar result computationally, we consider the following test case. The initial mass center positions are $(0.22, 0.125, 0.75)$ and $(0.78, 0.125, 0.75)$, respectively. The frames rigidly

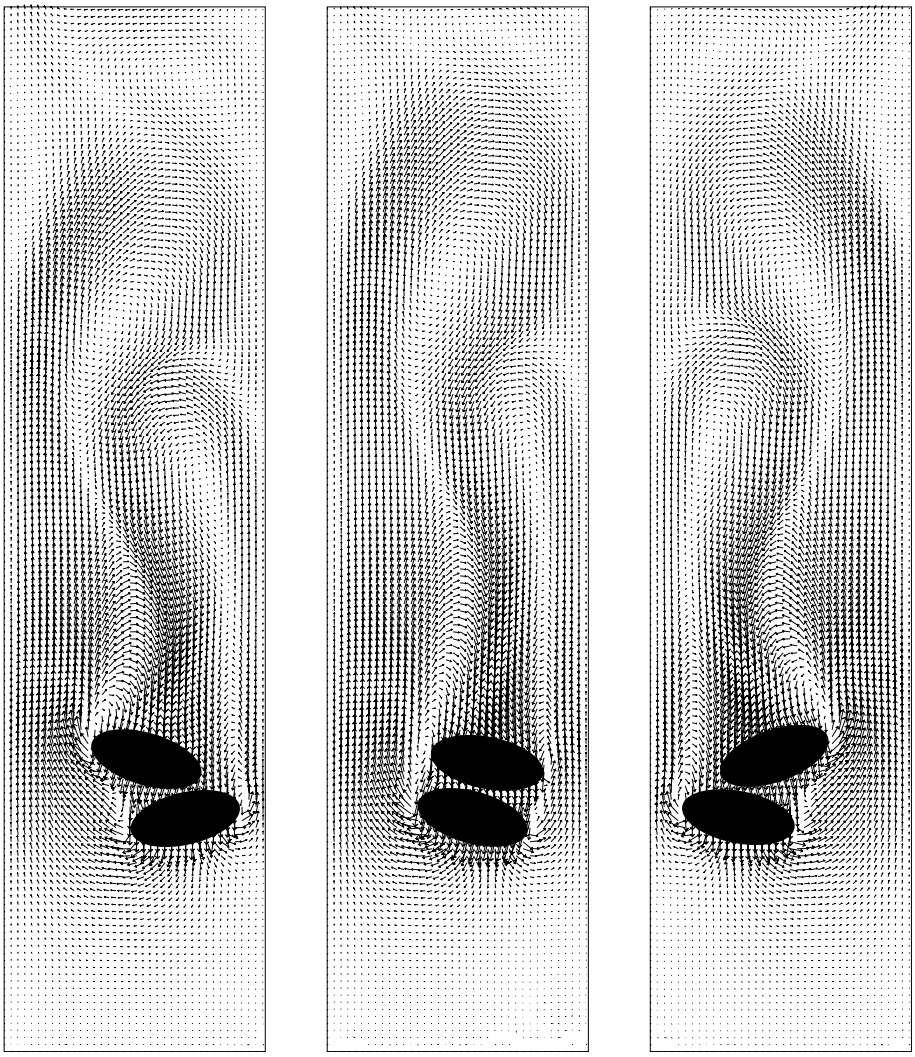

Fig. 12. Velocity field at $t = 4$, 5 and 9 on the plane passing through the mass center of the top ellipsoid for the case of density 1.25 and long semi-axis 0.22 (from left to right).

attached to the ellipsoids are $\{(\cos\frac{\pi}{3}, 0, \sin\frac{\pi}{3})$, (0,1,0), $(\cos\frac{5\pi}{6}, 0, \sin\frac{5\pi}{6})\}$ and $\{(\cos(\frac{-\pi}{3}), 0, \sin(\frac{-\pi}{3}))$, $(0,1,0)$, $(\cos\frac{\pi}{6}, 0, \sin\frac{\pi}{6})\}$ initially, respectively (see the position of ellipsoids at $t = 0$ in Fig. 7). The long semi-axis is 0.18 and $\{h_v,\Delta t\}$ is $\{1/112, 0.001\}$. All other parameters are same as in the previous case. The averaged terminal speed of two ellipsoids is 1.66 obtained for the last five periods of oscillation, so the averaged particle Reynolds number is 59.76 based on the length of the long axis (which is 0.36). Positions of two ellipsoids similar to those in Fig. 6 are shown in Fig. 7. It is in good qualitative agreement with experimental results. The period of the motion is 0.39 s. As shown in Fig. 8, we have observed a strong interaction between two settling ellipsoids of long axis 0.36. Three snapshots of the velocity field projected on the plane passing through the mass center of the left ellipsoid are shown in Fig. 9. The velocity field is about symmetric with respect to the centerline. We believe that the jet stream between two ellipsoids when they become closer is one of the key factors for the oscillation we have observed. To see the effect of the length of the long axis and the density of the ellipsoid, we have considered two following tests. When only reducing the long axes to 0.32 and keeping other parameters unchanged from the above case, they settle side-by-side in the channel with a weak interaction of period 0.3856 s. When increasing the density to 1.25 and keeping other parameters unchanged from the above case, the interaction of two ellipsoids becomes stronger and faster with period 0.2472 s. The histories of the horizontal position of the mass center of both cases are shown in Fig. 8. The memory used in the simulation is

about 186 Mb for $h_v = 1/112$. The simulation takes about 43 s per time step for $(h_v, \Delta t) = \{1/112, 0.001\}$ on a Linux based PC with 1.6 GHz Athlon CPU.

4.3. One ellipsoid on top of another one

It had also been observed experimentally by Joseph et al. that two cylinders with round ends can move around each other and stay together while they are settling down in the channel. It is unlike the case for two balls settling in a Newtonian fluid, which is known as drafting, kissing, and tumbling [38]. Two balls always break away after tumbling.

In this test case all parameters are same as in Section 4.1 except those mentioned in the following. The initial mass center positions are (0.5, 0.125,0.9) and (0.5,0.125,1.25), respectively, so one is on top of the other. The long axes of both ellipsoids are parallel to the x–axis initially. Two short semi-axes of both ellipsoids are 0.1. The ellipsoid density is $\rho_s = 1.25$ and $\{h_v,\Delta t\}$ is $\{1/112,0.001\}$. To study the effect of the long axis to the interaction between two ellipsoids, we have considered three cases with long semi-axes 0.21, 0.22 and 0.23, respectively.

The averaged terminal speeds of two ellipsoids are 4.847, 4.818 and 4.81 for the long semi-axes 0.21, 0.22 and 0.23, respectively, for the last 2 s. The averaged particle Reynolds numbers are 203.574, 211.992 and 221.26 based on the long semi-axes 0.21, 0.22 and 0.23, respectively. We have observed that two ellipsoids always interact with each other and stay together. The snapshots of the position of two ellipsoids are shown in Fig. 10 for the case of long semi-axis 0.22. In Fig. 11, the histories of the x-coordinate of the mass centers of two ellipsoids are shown. We have observed that for ellipsoids of long semi-axes 0.21 they interact at one side of channel and for ellipsoids of long semi-axes 0.23 they interact more chaotically and oscillate between two sides. Somewhere around 0.22 is the critical length of long semi-axis for them to start oscillating between two sides of the channel. Snapshots of the velocity field projected on the plane passing through the mass center of the top ellipsoid are shown in Fig. 12 for the case of long semi-axes 0.22. The memory used in the simulation is about 186 Mb for $h_v = 1/112$. It takes about 25 s per time step on a Linux based PC with 2.2 GHz AMD Opteron 64-bit CPU.

Acknowledgement

We acknowledge the helpful comments and suggestions of R. Bai, E.J. Dean, J. He, H.H. Hu, P.Y. Huang, G.P. Galdi, Y. Kuznetsov, V. Paulsen, J. Periaux and referees. We acknowledge also the support of NSF (grants ECS-9527123, CTS-9873236, DMS-9973318, CCR-9902035, DMS-0209066), and DOE/LASCI (grant R71700K-292-000-99).

References

[1] Liu YJ, Joseph DD. Sedimentation of particles in polymer solutions. J Fluid Mech 1993;255:565–95.
[2] Hu HH, Joseph DD, Crochet MJ. Direct simulation of fluid particle motions. Theor Comput Fluid Dynam 1992;3:285–306.
[3] Ladd AJC. Numerical simulations of particulate suspensions via a discretized Boltzmann equation, Part 1. Theoretical foundation. J Fluid Mech 1994;271:285–310.
[4] Ladd AJC. Numerical simulations of particulate suspensions via a discretized Boltzmann equation, Part 2. Numerical results. J Fluid Mech 1994;271:311–40.
[5] Hu HH. Direct simulation of flows of solid-liquid mixtures. Int J Multiphase Flow 1996;22:335–52.
[6] Johnson A, Tezduyar T. 3-D simulation of fluid-rigid body interactions with the number of rigid bodies reaching 100. Comput Meth Appl Mech Engrg 1997;145:301–21.
[7] Maury B, Glowinski R. Fluid-particle flow: a symmetric formulation. CR Acad Sci Paris 1997;324(Série 1): 1079–84.
[8] Hofler K, Muller M, Schwarzer S, Wachman B. Interacting particle-liquid systems. In: Krause E, Jager W, editors. High Performance Computing in Science and Engineering. Berlin: Springer-Verlag; 1998.
[9] Glowinski R, Pan TW, Hesla T, Joseph DD. A distributed Lagrange multiplier/fictitious domain method for flows around moving rigid bodies: application to particulate flows. Int J Multiphase Flow 1999;25:755–94.
[10] Glowinski R, Pan TW, Hesla T, Joseph DD, Périaux J. A fictitious domain approach to the direct numerical simulation of incompressible viscous flow past moving rigid bodies: application to particulate flow. J Comput Phys 2001;169:363–426.
[11] Takagi S, Ogz HN, Zhang Z, Prosperetti A. PHYSALIS: A new method for particle simulation. Part II: Two-dimensional Navier–Stokes flow around cylinders. J Comput Phys 2003;187:371–90.
[12] Dong S, Liu D, Maxey M, Karniadakis GE. Spectral distributed multiplier (DLM) method: algorithm and benchmark test. J Comput Phys 2004;195:695–717.
[13] Juárez LH, Glowinski R, Pan TW. Numerical simulation of the sedimentation of rigid bodies in an incompressible viscous fluid by Lagrange multiplier/fictitious domain methods combined with the Taylor–Hood finite element approximation. J Sci Comput 2002;17:683–94.
[14] Rugonyi S, Bathe KJ. On finite element analysis of fluid flows fully coupled with structural interactions. Comput Model Engrg Sci 2001;2:195–212.
[15] Bathe KJ, Zhang H. Finite element development for general fluid flows with structural interactions. Int J Numer Meth Fluids 2004;60:213–32.
[16] Glowinski R, Hesla T, Joseph DD, Pan TW, Périaux J. Distributed Lagrange multiplier methods for particulate flows. In: Bristeau MO, Etgen G, Fitzgibbon W, Lions JL,

Périaux TS, Wheeler MF, editors. Computational Science for the 21st Century. Chichester: J. Wiley.

[17] Glowinski R, Pan TW, Hesla T, Joseph DD, Périaux J. A fictitious domain method with distributed Lagrange multipliers for the numerical simulation of particulate flow. In: Mandel J, Farhat C, Cai XC, editors. Domain Decomposition Methods 10. Providence: American Mathematical Society; 1998.

[18] Glowinski R, Pan T-W, Hesla T, Joseph DD, Périaux T. A distributed Lagrange multiplier/fictitious domain method for flow around moving rigid bodies: application to particulate flow. Int J Numer Meth Fluids 1999;30: 1043–66.

[19] Baaijens FPT. A fictitious domain/mortar element method for fluid–structure interaction. Int J Numer Meth Fluids 2001;35:743–61.

[20] Wagner GJ, Moes N, Liu WK, Belytschko T. The extended finite element method for rigid particles in Stokes flow. Int J Numer Meth Engrg 2001;51:293–313.

[21] Yu Z, Phan-Thien N, Fan Y, Tanner RI. Viscoelastic mobility problem of a system of particles. J Non-Newtonian Fluid Mech 2002;104:87–124.

[22] Pan TW, Joseph DD, Bai R, Glowinski R, Sarin V. Fluidization of 1204 spheres: simulation and experiments. J Fluid Mech 2002;451:169–91.

[23] Pan TW, Joseph DD, Glowinski R. Modeling Rayleigh–Taylor instability of a sedimenting suspension of several thousand circular particles in a direct numerical simulation. J Fluid Mech 2001;434:23–37.

[24] Maury B. A many-body lubrication model. CR Acad Sci Paris 1997;325(Série 1):1053–8.

[25] Peskin CS. Numerical analysis of blood flow in the heart. J Comput Phys 1977;25:220–52.

[26] Peskin CS, McQueen DM. Modeling prosthetic heart valves for numerical analysis of blood flow in the heart. J Comput Phys 1980;37:113–32.

[27] Peskin CS. Lectures on mathematical aspects of physiology. Lect Appl Math 1981;19:69–107.

[28] Glowinski R. Finite element methods for the numerical simulation of unsteady incompressible viscous flow modeled by the Navier–Stokes equations. In: Ciarlet PG, Lions JL, editors. Handbook of Numerical Analysis, vol. IX. Amsterdam: North-Holland; 2003.

[29] Chorin AJ, Hughes TJR, Marsden JE, McCracken M. Product formulas and numerical algorithms. Comm Pure Appl Math 1978;31:205–56.

[30] Marchuk GI. Splitting and alternating direction methods. In: Ciarlet PG, Lions JL, editors. Handbook of Numerical Analysis, vol. I. Amsterdam: North-Holland; 1990.

[31] Pan TW, Glowinski R, Galdi GP. Direct simulation of the motion of a settling ellipsoid in Newtonian fluid. J Comput Appl Math 2002;149:71–82.

[32] Glowinski R, Pan TW, Périaux J. Distributed Lagrange multiplier methods for incompressible flow around moving rigid bodies. Comput Meth Appl Mech Engrg 1998;151: 181–94.

[33] Adams J, Swarztrauber P, Sweet R. FISHPAK: A Package of Fortran subprograms for the Solution of Separable Elliptic Partial Differential Equations. Boulder, CO: The National Center for Atmospheric Research; 1980.

[34] Dean EJ, Glowinski R. A wave equation approach to the numerical solution of the Navier–Stokes equations for incompressible viscous flow. C R Acad Sci Paris 1997; 325(Série 1):783–91.

[35] Dean EJ, Glowinski R, Pan TW. A wave equation approach to the numerical simulation of incompressible viscous fluid flow modeled by the Navier–Stokes equations. In: De Santo JA, editor. Mathematical and Numerical Aspects of Wave Propagation. SIAM: Philadelphia; 1998.

[36] E. Rimon, S. Boyd, Efficient distance computation using best ellipsoid fit, The IEEE International Symposium on Intelligent Control, Glasgow, UK, IEEE, 1992.

[37] Chou JCK. Quaternion kinematic and dynamic differential equations. IEEE Trans Robotics Automat 1992;8:53–64.

[38] Fortes AF, Joseph DD, Lundgren TS. Nonlinear mechanics of fluidization of beds of spherical particles. J Fluid Mech 1987;177:467–83.